# The present status in super-heavy element calculations

Damgaard, Jakob; Nilsson, Sven Gösta

*Published in:*
Physica Scripta

1972

# Physica Scripta

A monthly journal published by

**THE ROYAL SWEDISH ACADEMY OF SCIENCES**



---

S. G. Nilsson and J. Damgaard

**The Present Status in Super-heavy Element Calculations**

---

**Reprint from**

Vol. 6 1972 No. 2-3

The Almqvist & Wiksell Periodical Company, Stockholm, Sweden

Physica Scripta. Vol. 6, 81–93, 1972

# The Present Status in Super-heavy Element Calculations

S. G. Nilsson and J. Damgaard

Department of Mathematical Physics, Lund Institute of Technology, Lund, Sweden

*Received August 18, 1972*

**Abstract**

*The present status in super-heavy element calculations.* S. G. Nilsson and J. Damgaard (Department of Mathematical Physics, Lund Institute of Technology, Lund, Sweden).
*Physica Scripta* (*Sweden*) *6*, 81–93, 1972.

The theoretical work done in predicting a possible island of super-heavy elements with masses centered around A about 300, or about 15 % in excess of the heaviest elements presently synthesized, is reviewed. Both the Hartree–Fock and the single-particle shell model approaches are discussed, with particular emphasis on the latter. The convergence in predictions of independent theoretical research groups is noted.

## 1. Introduction

The subject of the fission decay and the determination of half-lives of heavy and super-heavy elements (SHE) has recently been reviewed in considerable detail by Johansson, Nilsson and Szymanski in Ann. de Phys. [1], by Brack, Damgaard, Pauli, Jensen, Strutinsky and Wong in Rev. Mod. Phys. [2], and most recently by J. R. Nix in Ann. Rev. of Nucl. Sci. [3].

The most complete methodological discussion is contained in the second reference while the third paper contains the most complete reference list. In view of the availability of these sources we shall exclude a historical survey of the subject and confine ourselves to some rather recent details and some evaluation of the relative merits of the different approaches followed.

## 2. The two-body force approach

In Fig. 1 we exhibit the peninsula of known elements relative to the conceived island of stability connected with $Z=114$, $N=184$. The most satisfactory way a priori to bridge our knowledge gap associated with the channel of instability separating the island from the peninsula is to employ our knowledge of the nucleon–nucleon two-body interaction.

This approach is in the long-range view the most promising. Presently there exist at least two competing variants of this approach. One is to employ a near-realistic two-body interaction such as that of Tabakin. This is the line of approach followed by Bassichis, Kerman and Wilets and their co-workers [4]. The other, which in the intermediate-time-range perspective appears the most successful one, is to employ an effective force fitting nuclear matter properties as well as some well-established single-particle level schemes (in particular is the spin-orbit strength determined from such a fit). This is the line followed by Vauterin et al. [5] and Köhler [6]. The success of the latter method is reflected in the good spherical as well as deformed single-particle orbitals obtained [7]. However, it seems difficult at present to extrapolate this type of calculation in a reliable way. This difficulty is reflected in the rather different spectra

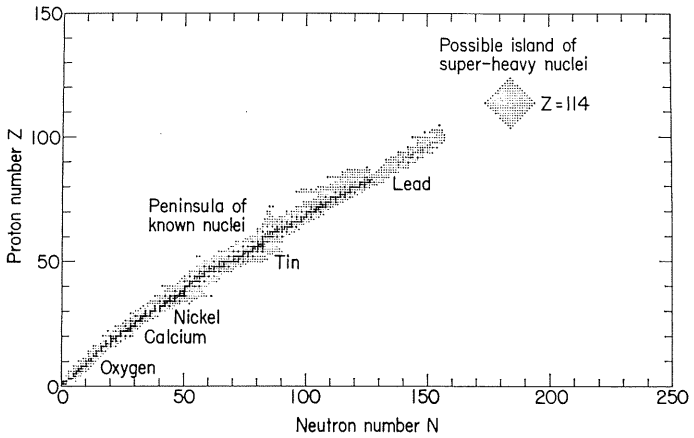


*Fig. 1.* Peninsula of known nuclei and the possible island of predicted super-heavy nuclei connected with $Z=114$. Heavy and light points mark elements with known half-lives greater and smaller than 1 year. (Courtesy Ray Nix.)

obtained in the calculations of Vauterin et al. and the very similar calculations of Köhler. The comparison is exhibited in Figs. 2 and 3, where to the left in the figures one also sees the extrapolated single-particle schemes according to the Lund–Berkeley–Warsaw [1], Los Alamos [3] and Moscow–Copenhagen–Basle [2] groups, respectively.

At present, the aim of these Hartree–Fock calculations of the Vauterin–Vénéroni–Brink group appears to be the very sound one of first requiring a good fit to experiments in some well-established deformed regions.

The next step is the reproduction of the fission barrier as to its basic feature, the two-peak shape and the secondary minimum. Once these goals are achieved, one will be ready for a systematic assault on the SHE region.

Some calculations have been performed in the $^{134}$Ce region. These initially had the intention of trying to reproduce a secondary minimum at $\varepsilon \simeq 0.5$–$0.6$ for which there may exist some weak experimental indication. The calculations by Vauterin et al., however, fail to give any such secondary minimum. This is also in agreement with the results of the calculations by Ragnarsson [8] based on the Strutinsky shell correction method. As a preliminary conclusion it seems fair to say that the Hartree–Fock calculations support the stiff character of the liquid-drop energy surface in the $A \simeq 130$ region even quantitatively.

The advantage of the Hartree–Fock approach is that for the extremal points of the potential-energy surface all the relevant degrees of freedom are automatically included, provided the model space taken is large enough. Between extremal points one studies the auxiliary Hamiltonian

$$H' = H - \lambda(Q - Q_0)^2$$

Thus, the potential energy is investigated for every given $Q_0$-value. In this way one obtains a fission path which automatically

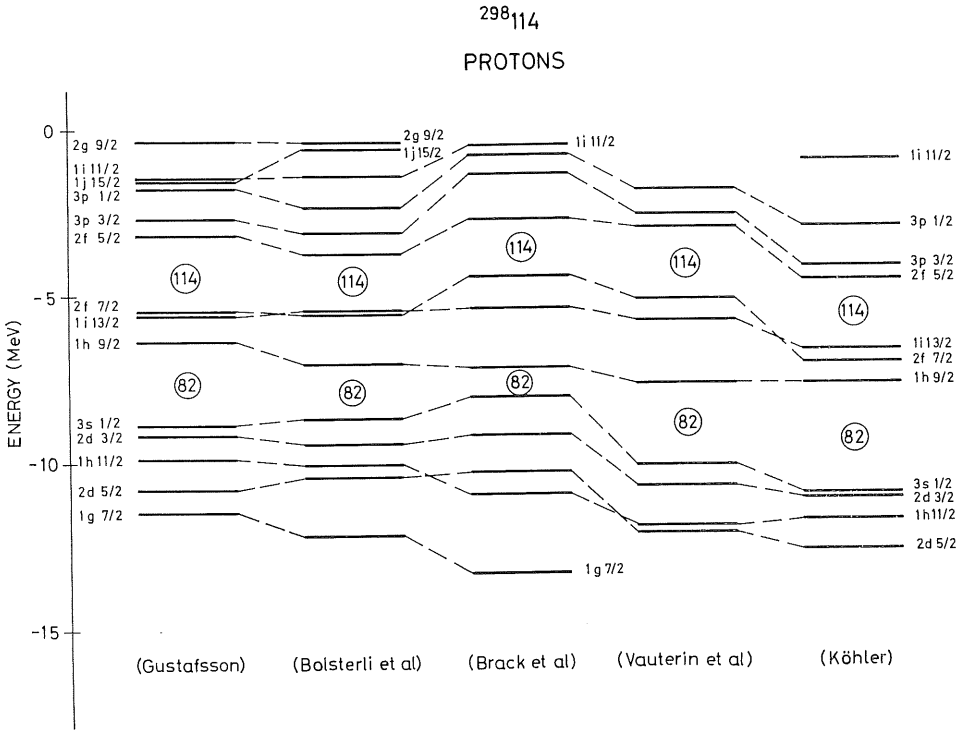


*Fig. 2.* Single-proton orbitals for spherical shapes for $A \simeq 300$. Farthest to the left is exhibited the predictions of the modified h.o. model [9] next the predicted level scheme according to M. Bolsterli et al. [34] and M. Brack et al. [2], respectively. These three level schemes represent some of the most frequently employed single particle models. The two right level schemes are obtained in calculations with two-body interactions by D. Vauterin et al. [5] and by S. Köhler [6]. (Figure taken from ref. [1].)

includes other degrees of freedom, though in a static fashion. This method thus in this feature resembles the path projection method used in ref. [9].

### 3. The microscopic–macroscopic approach

The idea of a microscopic-macroscopic method was proposed by Swiatecki [10], but in its present workable form this approach was developed by Strutinsky [11]. In connection with the foregoing section it should also be mentioned that Strutinsky and his co-workers [12] recently have attempted to establish a link between the microscopic-macroscopic approach and the theory of Fermi liquids.

In contrast to the situation in the Hartree–Fock calculations the definition of deformation coordinates becomes—as we shall see—a crucial point in this method. For an idea of the shapes involved in the fission of nuclei in the actinide region (see Fig. 4).

As this method is based on a shell-model potential, another problem is that of determining the radial shape and the spin-orbit component of the nuclear one-body potential. As for the radial shape, the potentials employed in refs. [2] and [3] are probably preferable to the alternatives suggested for the spontaneous fission problem. The $I^2$-term of ref. [9] seems, however, to give rise to a radial density distribution very similar to that generated by the Woods–Saxon type potentials.

For investigations near and particularly beyond the scission

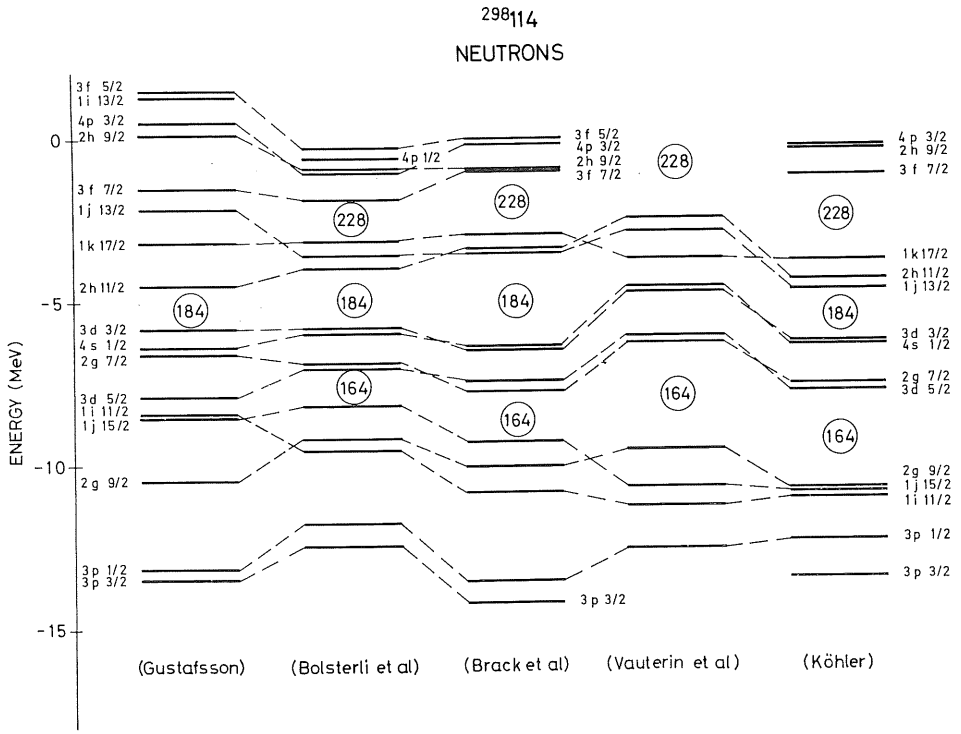


*Fig. 3.* Same as Fig. 2 but for neutron levels. Note the large $N=184$ gap predicted by M. Brack et al. [2] and the very small $N=184$ gap in the calculations by D. Vauterin et al. [5]. In the latter calculations instead $N=228$ assumes a similar role. The gap $N=228$ is also large in the S. Köhler [6] calculations. (Figure taken from ref. [1].)

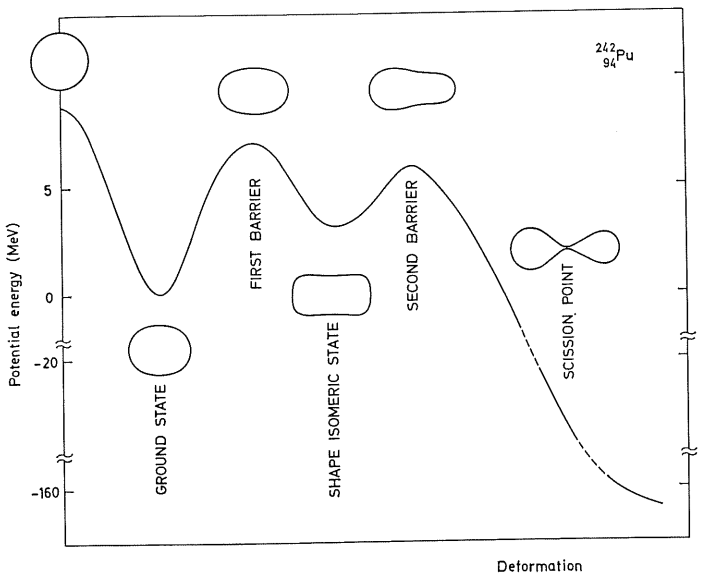


*Fig. 4.* The nuclear fission barrier as a function of deformation. Realistic deformation shapes are indicated in the figure above and below the barrier curve.

point, two-center potentials may be preferable. Some two-center formulations for axially symmetric nuclei using an oscillator with a bump added along the symmetry axis, or two joined oscillators, have been proposed by Andersen et al. [13], Greiner and co-workers [14], Johansson [15] and Slavov et al. [16]. All have their advantages, in particular over the one-center modified oscillator potential, when one approaches the scission point. For more modest distortions, sufficient to describe actinide and SHE fission barriers out to the exit point, we believe the generalised oscillator discussed here is still very satisfactory.

Before we proceed with the problem of the single-particle potential, let us consider for a moment two other central problems in the microscopic-macroscopic approach.

The total energy of a nucleus is to be calculated as a smooth liquid-drop energy supplemented by a term representing shell structure. The latter is the sum of the real single-particle energies minus a background of smeared energy levels.

$$E_{\text{shell}} = \Sigma e_\nu - \langle \Sigma e_\nu \rangle$$

A central problem is how this background is to be estimated. Bohr and Mottelson [17] in the preliminary version of vol. II of their monograph consider three avenues, alternative to the use of the Strutinsky smearing function.

1. Let $A \to \infty$ and try to isolate smooth terms proportional to $A$, $A^{2/3}$, $A^{1/3}$ etc. What remains after the subtraction of these gross structure terms is the shell correction term.

2. *$T$ large.* For sufficiently large temperature $T$, the total energy or, even better, the entropy becomes a smooth function of $T$, which can be extrapolated back to $T=0$. The difference between actual and extrapolated energies is the shell-correction energy. Such a method has also been considered by others [18] and for higher energies some reservations have been raised against it [19]. Shell energies obtained in this way by R. Bengtsson [20] are compared with shell-energies obtained by the shell-correction method in Figs. 5*a* and 5*b*.

3. Let *$\varepsilon$ be large.* By a study of the summed single-particle energies as functions of $\varepsilon$ one should be able to isolate the long-range behaviour of e.g. the shell correction and surface energy terms.

A combination of 1 and 3 has also been suggested earlier by Swiatecki and Tsang [21].

Methods 1 and 2 are at present being studied in Lund and Copenhagen. It appears that the applicability of 1 for the modified oscillator potential is dependent on the prescribed behaviour of the $\varkappa$ and $\mu$ coefficients (multiplying $\boldsymbol{l}\cdot\boldsymbol{s}$ and $\boldsymbol{l}^2$) at large $A$-values and therefore the method is less useful in this case.

These alternative methods may from a physical viewpoint appear more attractive than that suggested by Strutinsky. The method developed by him remains for the moment the most explored and probably therefore the safest. Given $E_{\text{shell}}$ one finally obtains the total energy $W$ as

$$W = E_{\text{shell}} + E_{\text{pair}} + E_{\text{surf}} + E_{\text{coul}}$$

i.e. by adding to $E_{\text{shell}}$ a pairing correction term, a surface energy term and a Coulomb term, the latter two terms representing the liquid-drop contributions. In obtaining $E_{\text{shell}}$ we have thus used the Strutinsky method and in the following we shall limit ourselves to calculations performed on this basis.

There remains to be said a few words about the problem of the liquid-drop terms. The corresponding coefficients are usually taken from the Lysekil version [22] of the Myers–Swiatecki ground state mass and actinide barrier fits.

Relative to that of spherical shape the liquid-drop energy of a given shape can be written as [3]

$$E_{\text{l.d.}} = \{[B_s\ (\text{shape}) - 1] + 2x\,[B_c\ (\text{shape}) - 1]\}E_s^{(0)}$$

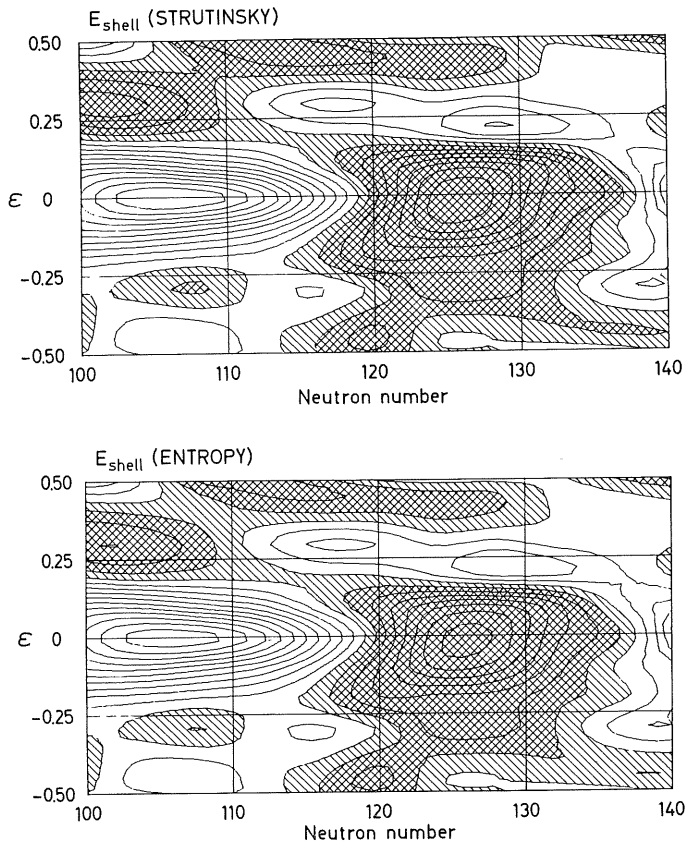


*Fig. 5a.* The neutron shell energy calculated for the modified-oscillator model according to the method suggested by Strutinsky as a function of distortion $\varepsilon$ and neutron number $N$. (Private communication from Ragnar Bengtsson.)

*Fig. 5b.* The neutron shell energy as obtained by the temperature method (see text) in the same ranges of $\varepsilon$ and $N$ as in Fig. 5*a*. (Private communication from Ragnar Bengtsson.)

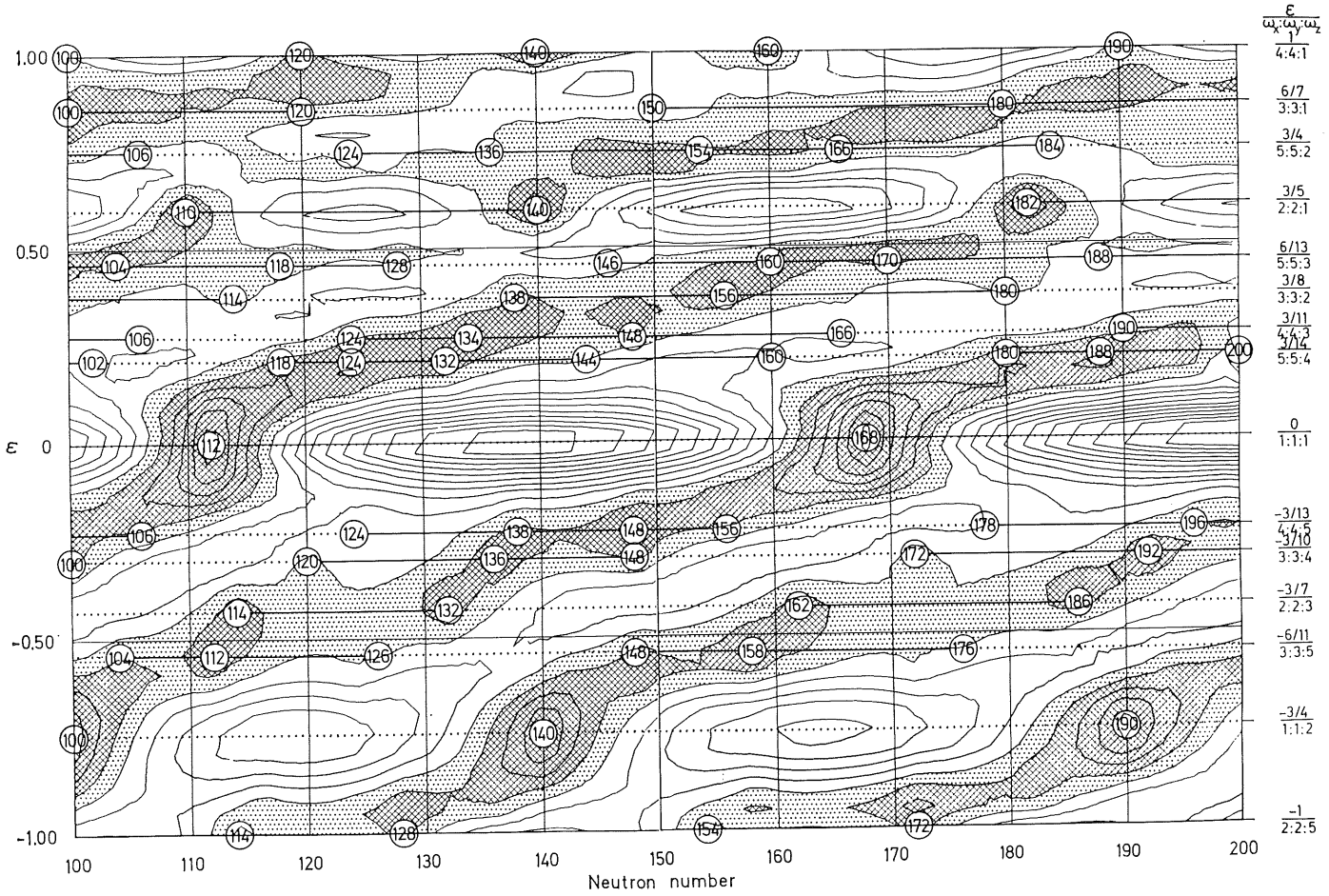


*Fig. 6.* Neutron shell-energy $\Sigma e_\nu - \langle \Sigma e_\nu \rangle$ for the pure harmonic oscillator exhibiting valleys and mountain ridges, the former reflecting closed shell nucleon numbers corresponding to rational axis ratios, as indicated to the right in the figure. Note in particular the magic numbers $N=140$ and $N=182$ for $\varepsilon=0.6$ on the prolate side and $N=140$, 190 for $\varepsilon=-0.75$ on the oblate side. The contour line separation is 3 MeV. (Private communication from Ragnar Bengtsson.)

where $B_s$ (shape) and $B_c$ (shape) are the relative shape contributions to the surface and Coulomb energies, respectively. The surface energy of a spherical nucleus is given by

$$E_s^{(0)} = a_s\left(1-\varkappa_s\left(\frac{N-Z}{A}\right)^2\right)A^{\frac{2}{3}}$$

and the fissility parameter

$$x = \frac{E_c^{(0)}}{2E_s^{(0)}} = \frac{Z^2/A}{(2a_s/a_c)\left(1-\varkappa_s\left(\frac{N-Z}{A}\right)^2\right)}$$

The corresponding parameters were listed by Myers and Swiatecki as

$a_s = 17.9439$ MeV

$a_c = 0.7053$ MeV (or $r_0 = 1.2249$ fm)

$\varkappa_s = 1.7826$ (or equal to the corresponding coefficient in the volume energy)

## 4. One single-particle potential

To become a little more specific, we start from the following type of potential, the modified harmonic oscillator potential,

$$V = \tfrac{1}{2}\hbar\omega_0\varrho^2(1-\tfrac{2}{3}\varepsilon P_2 + 2\varepsilon_4 P_4 + 2\varepsilon_3 P_3 + 2\varepsilon_5 P_5) - 2\varkappa\hbar\omega_0 \boldsymbol{l}_t \boldsymbol{s} - \mu\varkappa\hbar\omega_0(l_t^2 - \langle l_t^2\rangle)$$

In this potential the $\varepsilon$ coordinate represents nuclear elongation, $\varepsilon_4$ waist-line development and $\varepsilon_3+\varepsilon_5$ reflection asymmetry. The potential is generalised below to include also axially asymmetric degrees of freedom.

Considering the $\varepsilon$-degrees of freedom only, one may study the shell correction energy $\Sigma e_\nu - \langle \Sigma e_\nu \rangle$ (see the preceeding section) as exhibited in Fig. 6 for the pure h.o. potential for neutron values between $N=100$ and $N=200$. (The corresponding $Z$-values are chosen to lie along the stability line.) The magic numbers connected with spherical shape are now $N=112$ and $N=168$. The corresponding numbers $N=110$, 140, 182 connected with $\varepsilon=0.6$ are clearly brought out in the middle of large valleys in the ($\varepsilon$, $N$) plane. A large number of other gap effects are apparent.

In Fig. 7 we exhibit the corresponding potential energy surface for the case that pairing as well as the correction terms proportional to $\boldsymbol{l}_t \boldsymbol{s}$ and $l_t^2$ are added to the modified oscillator potential. The spherical minima are now associated with $\varepsilon=0$ and $N=126$ and, much more weakly, $N=184$. Only the $N\simeq 140$ minimum is now clearly remaining associated with $\varepsilon=0.6$ though more shallow and also displaced to a somewhat larger $N$-value, or $N=148$.

This shell energy surface should be kept in mind when we consider the barriers below.

## 5. Other potentials

The two-center models may have their most valuable applications in the treatment of the heavy-ion collision problem. However, this

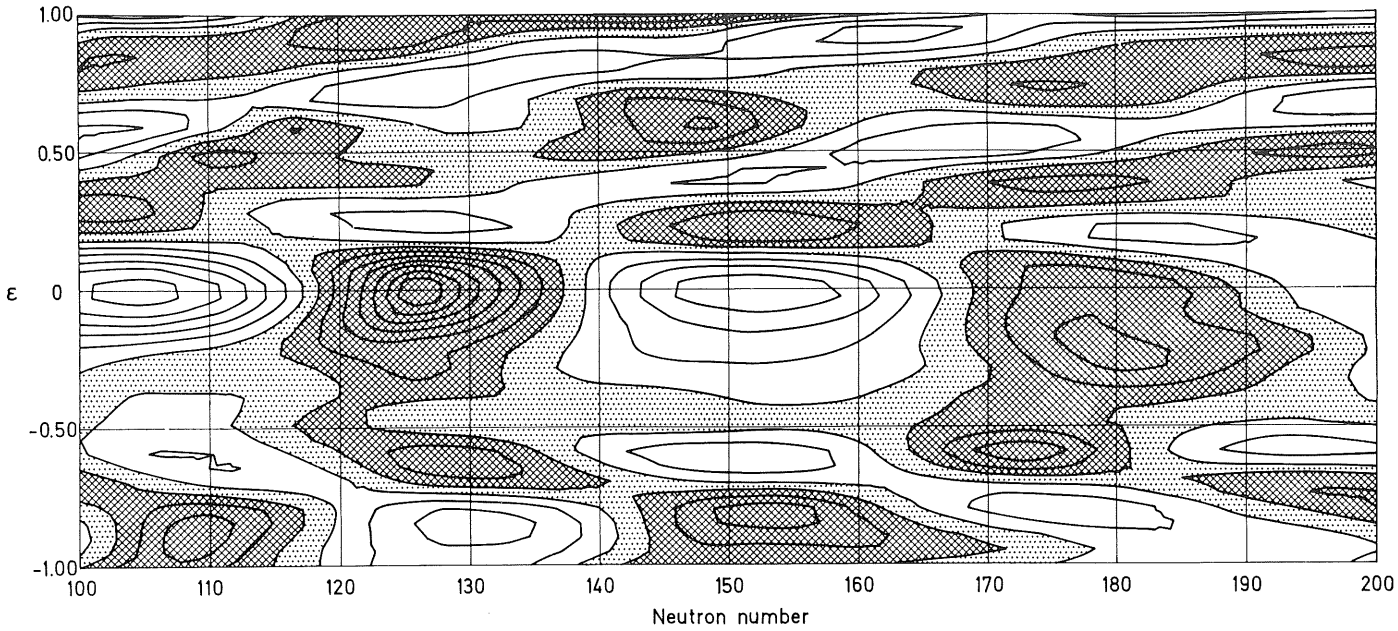


*Fig. 7.* Neutron shell plus pairing energy with $l_t$ $s$ and $l_t^2$ terms added under the assumption of the pairing matrix elements $G = \text{const}$. Contour line separation is here 1 MeV. The valleys and ridges of the previous figures are shifted by a few neutron numbers to slightly higher $N$-values. (Private communication from Ragnar Bengtsson.)

parametrisation has also shown its usefulness in the treatment of actinide and heavy rare-earth nuclei (see Fig. 8) [23]. Of great interest is also the ovaloid shape coordinates which are defined by the equation

$$(\varrho^2 + z^2)^2 + 2\varepsilon(\varrho^2 - z^2)\, R^2 + (\varepsilon^2 - 1)\, R^4 = 0$$

where to first order $\varepsilon$ has the same definition as in the spheroidal harmonic oscillator. The constant $R$ has to be determined from conservation of enclosed equipotential volumes. This parametrisation has then been applied to the harmonic oscillator and the Woods–Saxon potential by Pashkevich [24] and Adeev et al. [25].

One of the most satisfactory parametrisations for the middle and later stages of the fission process may be the parametrisation and radial shape used by Nix and co-workers [3]. Based on a set of pseudodensity shapes as given to the right in Fig. 9 a potential is generated by folding a Yukawa two-body-potential over these shapes as shown in Fig. 10. The resulting equipotential lines are exhibited to the right in Fig. 9, thus showing the desired two-center character for large waist-line distortions, but—and

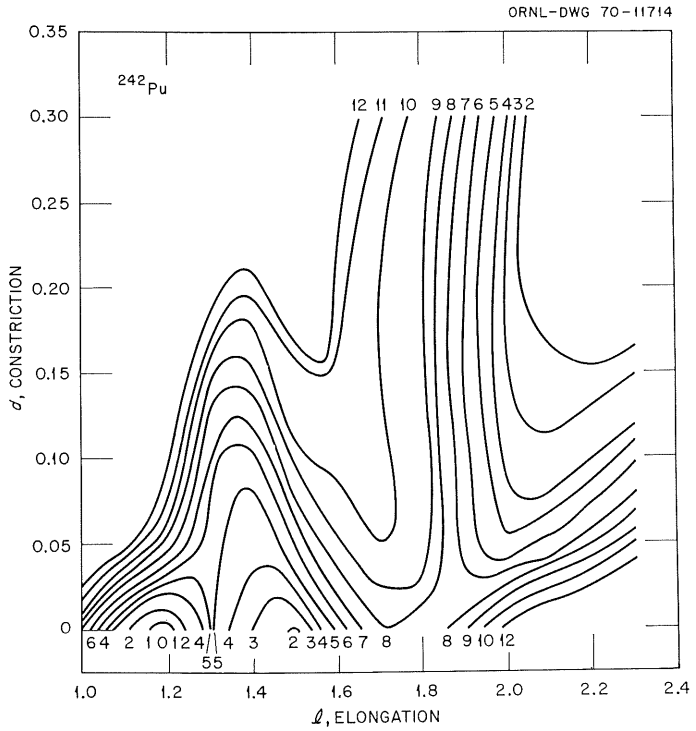


*Fig. 8.* Potential-energy surface calculated on the basis of the two-center potential by Mosel and Schmitt [23] plotted in terms of elongation and constriction. Note that minimum energy is obtained for a one-center shape all the way out to the second saddle point. Beyond that point the two-center coordinate appears to be of considerable importance.

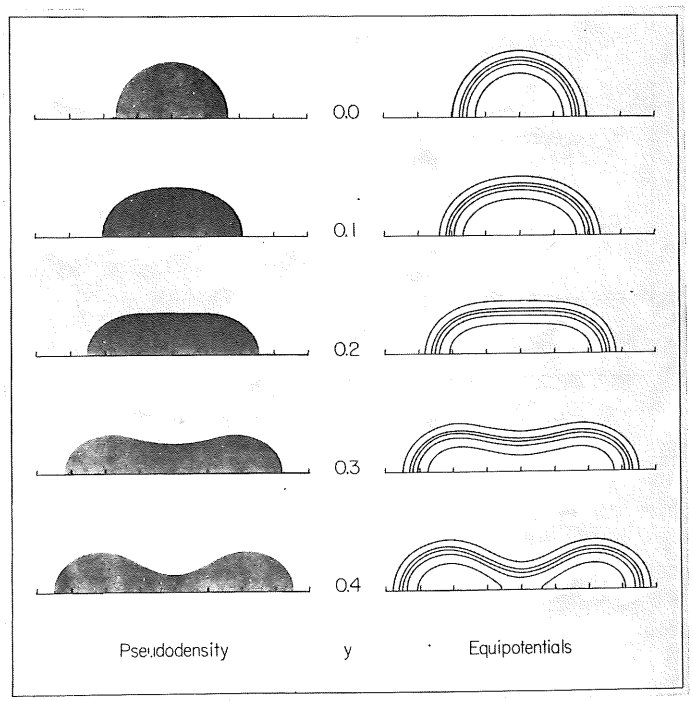


*Fig. 9.* The equipotential shapes corresponding to the potential used by Nix and coworkers [3]. Note that for a sufficiently deep central inscission a two-center type potential develops naturally.

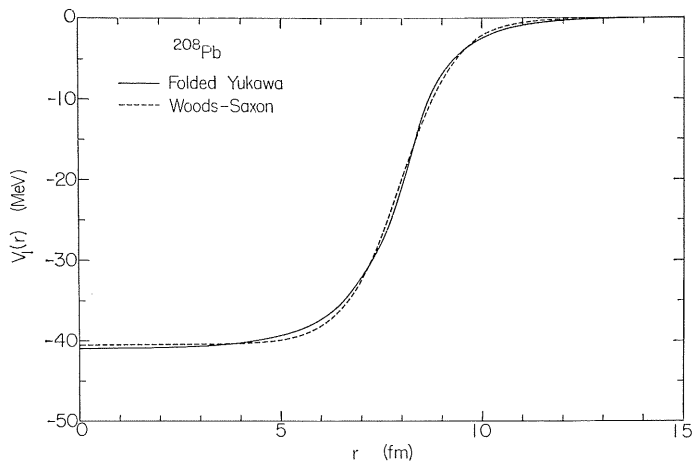


*Fig. 10.* Radial dependence of the potential employed by Nix and co-workers [8] compared with that of a Woods–Saxon potential.

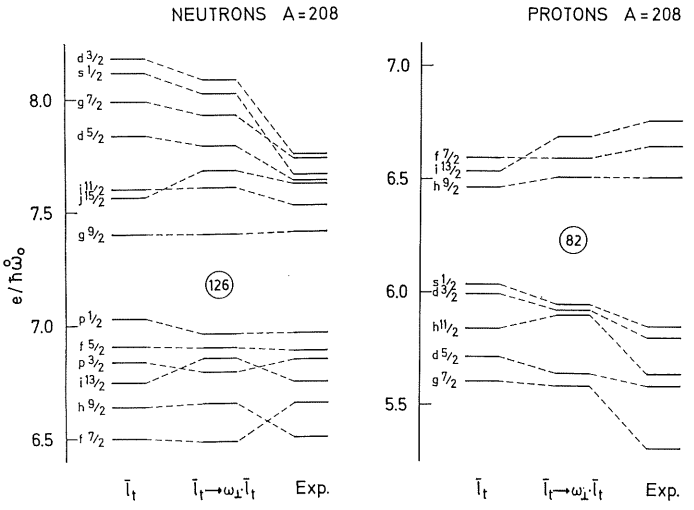


*Fig. 12.* Spherical neutron and proton single-particle levels for the modified harmonic oscillator potential as of ref. [9] to the left, in the middle the "scaled" version and to the right experiments. The comparison concerns mass regions near $A=208$. (Communication from R. Bengtsson.)

this is the advantage relative to two-center potentials—not for smaller ones.

The corresponding spin-orbit term is then generated according to the recipe $\sigma(\nabla V \times \boldsymbol{p})$. In this way the spin-orbit strength has a quadrupole dependence given a priori.

Very few complete single-particle diagrams are available for these Woods–Saxon type potentials but it appears that those which fit spherical nuclei, fit deformed ones less well with the same parameters. A critical study of the quadrupole shape dependence of the spin-orbit term is clearly called for.

At present it appears to us that the existing discrepancy as to the predicted shell spacings ("magic gaps") connected with the employment of the Woods–Saxon type potentials by the Nix and Strutinsky groups on one side and the generalised harmonic oscillator used by the Lund–Berkely–Warsaw group on the other largely depends on two facts. In the former case the fit is made primarily to spherical closed shell excitation spectra, while the modified harmonic oscillator has been fitted to the sequence of ground states of deformed nuclei. In the second place the discrepancy reflects the fact that the spin-orbit constant $\varkappa$ as well as $\mu$ is assumed to be independent of distortion in the modified oscillator case, while there is an $\varepsilon$-dependence prescribed a priori in the Woods–Saxon case.

Analysis of spectra in different spherical and deformed regions may be taken to indicate that at least $\varkappa$ is $\varepsilon$-dependent, consid-

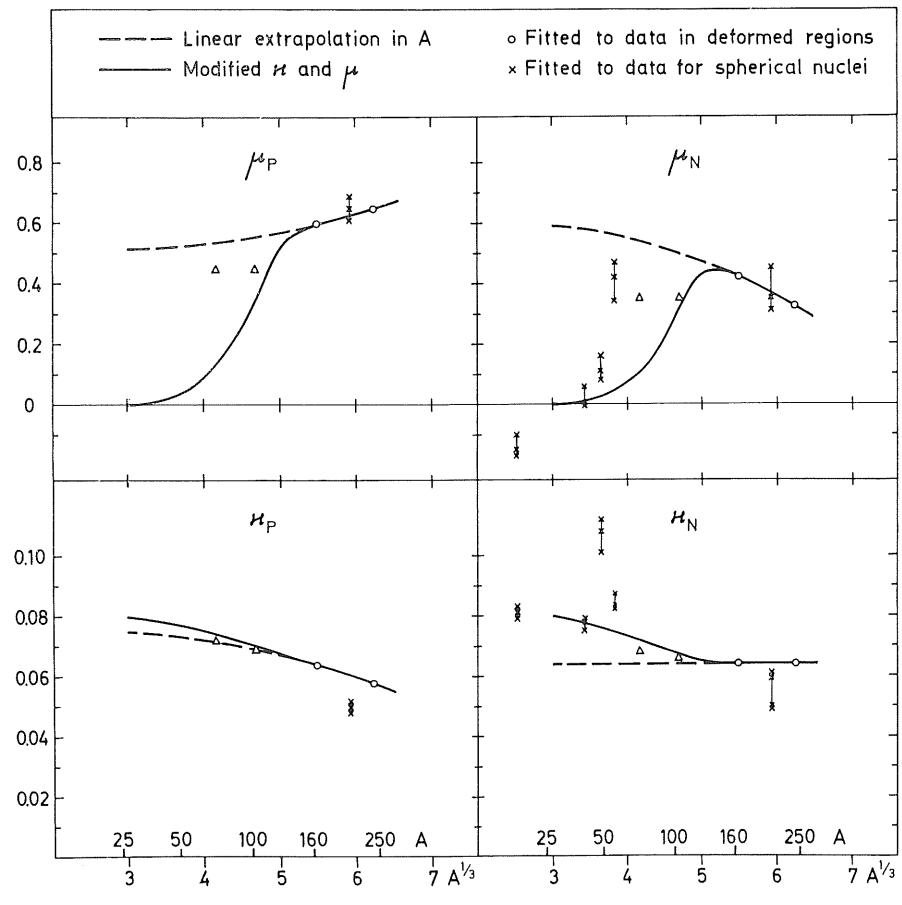


*Fig. 11.* The modified oscillator model parameters $\varkappa$ and $\mu$ for protons and neutrons, respectively, as functions of $A^{1/3}$. In the deformed regions ($A\simeq 165$ and $A\simeq 242$) the values have been chosen to fit the experimental energy levels as well as possible. The dashed lines indicate a linear extrapolation in $A$ based on the heavy deformed regions while, when the continuous lines have been drawn, we have somewhat arbitrarily taken the data for $A\approx 25$ into account. The crosses indicate least-square fits to spectroscopic data for closed shell $\pm 1$ nuclei near $^{16}$O, $^{40}$Ca, $^{48}$Ca, $^{56}$Ni and $^{208}$Pb. The three different crosses above each other indicate that alternative weights have been given to the different states in the single-particle spectra.

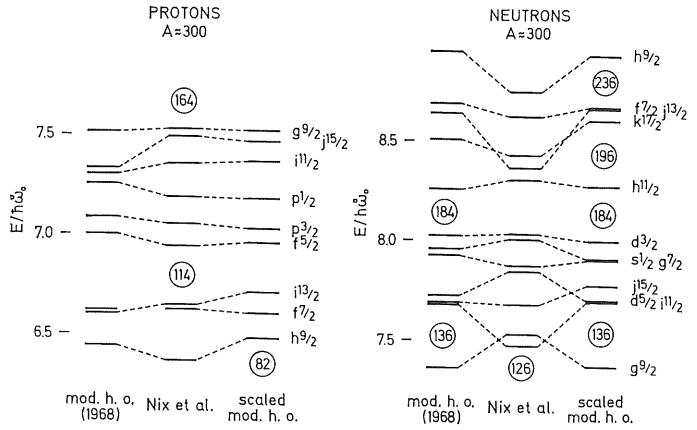


*Fig. 13.* Same as Fig. 12 for the mass region near $A=298$.

ering a linear $\varepsilon$-dependence, the coefficient of $\varepsilon$ seems to be about 1/3 (see Fig. 11).

Actually A. Bohr and B. Mottelson [17] suggest a distortion scaling of the modified oscillator potential in terms of $\varepsilon$ such that $x$ and $y$ are multiplied by $\omega_\perp/\omega_0$ while $z$ is multiplied by $\omega_z/\omega_0$. This leads to some new terms in the potential, but the dominant effect is that $\varkappa$ and $\mu$ are both multiplied by $\omega_\perp/\omega_0$, both are thus increasing with prolate and decreasing with oblate distortions. Similarly $\langle l^2\rangle_N$ is to be replaced by $[(n_\perp+1)\,\omega_\perp + (n_z+\frac{1}{2})\,\omega_z]^2/2\omega_0$. The consequences of this scale transformation are now being investigated in Lund. Preliminary findings seem to favour a change where only the $\boldsymbol{l}_t\,\boldsymbol{s}$ term is scaled while $\boldsymbol{l}_t^2-\langle \boldsymbol{l}_t^2\rangle$ is left unchanged. The resulting single-particle level diagrams in the Pb-region are shown to the left in Fig. 12 for the modified oscillator of ref. [9] and in the middle in the totally scaled case, as suggested by Bohr and Mottelson, while the empirical level order appears to the right. As before the fit is made to the deformed actinide single-particle level order in both of the theoretical cases.

The spherical $N=184$ gap is seen to be slightly increased in the "scaled" case, while the $Z=114$ gap is diminished (see Fig. 13). The agreement with e.g. the scheme of Nix et al. [3] is somewhat closer in the scaled case.

## 6. Results of calculations using $\varepsilon$, $\varepsilon_4$ shapes

Results obtained by Tsang and Nilsson et al. in 1968 for the potential energy surfaces for a few super-heavy elements are given in Figs. 14 *a–b*. The coordinates then employed only involve $\varepsilon$ and

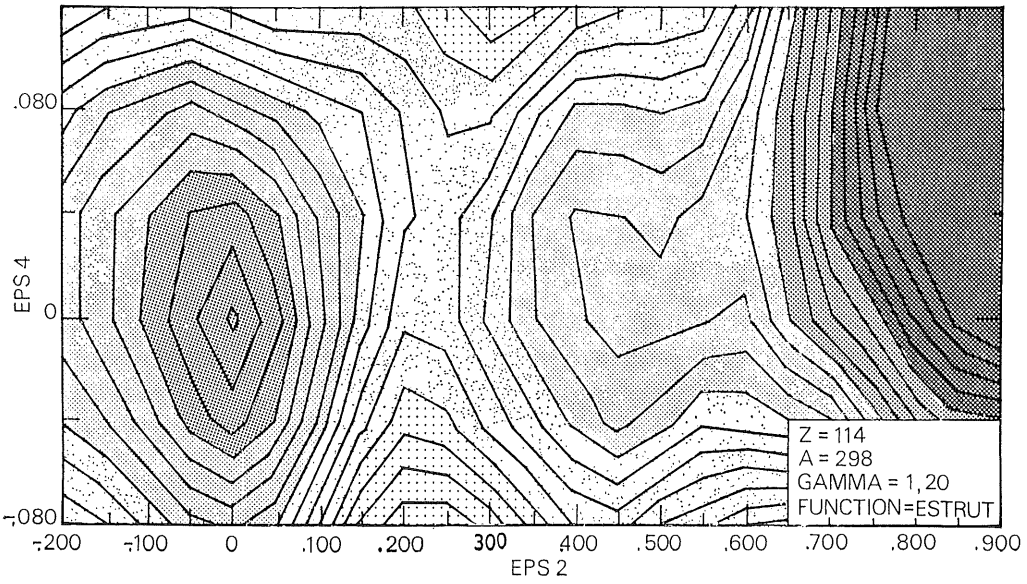


*Fig. 14a.* The potential-energy surface in $\varepsilon$, $\varepsilon_4$ for $^{298}114$ calculated in ref. [9]. (Figure taken from ref. [1].)

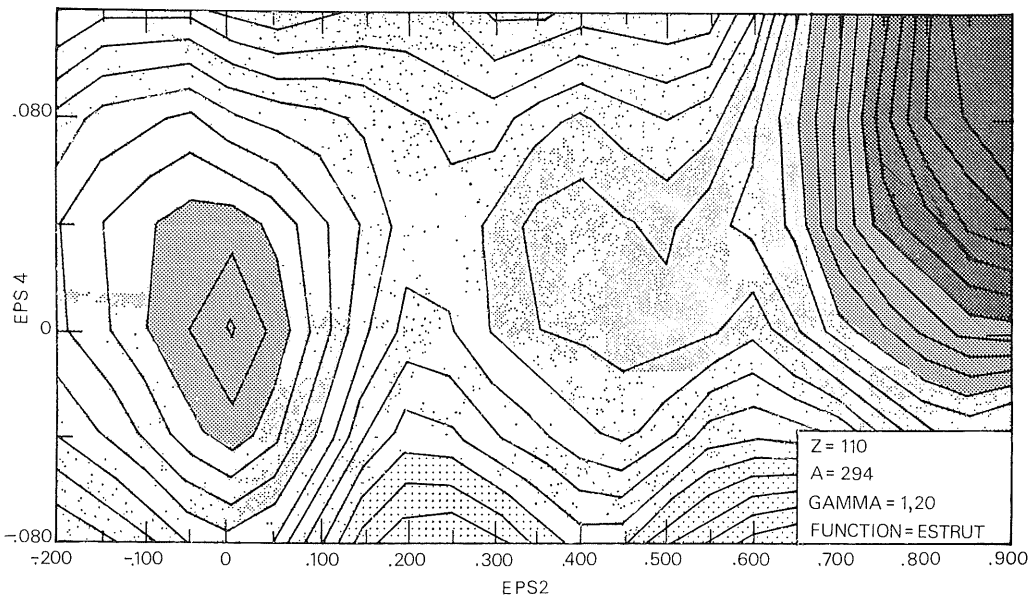


*Fig. 14b.* Same as Fig. 14*a* but for $^{294}110$. (Figure taken from ref. [1].)

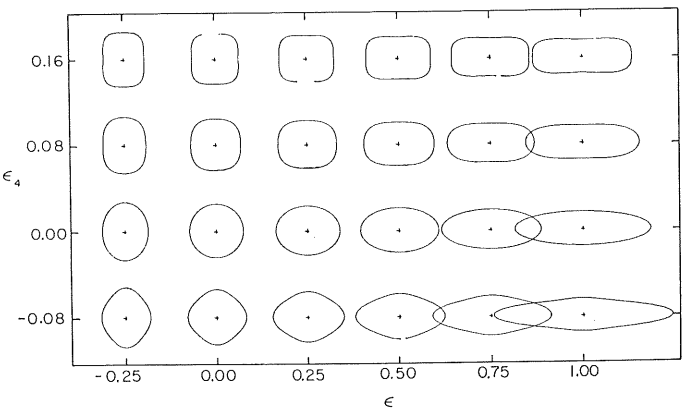


*Fig. 15.* The shapes generated by the set of values of $\varepsilon$ and $\varepsilon_4$ employed in ref. [9]. In the calculation of the potential energy we have found that one needs to employ a density of net points corresponding to $\Delta\varepsilon = 0.05$ and $\Delta\varepsilon_4 = 0.04$.

$\varepsilon_4$ coordinates. The shapes then considered are shown in Fig. 15.

Although the barrier exit corresponds to very modest distortions for the super-heavy element nuclei, a considerable fission barrier still remains because the ground state shape is spherical and not 20–30% distorted as for most actinide nuclei. The barrier of $^{298}114$ has a height and a half-life comparable to that of $^{242}$Pu.

## 7. The reflection-asymmetric degrees of freedom

We shall give a very short comment on the problem of the influence of the asymmetric coordinates along the fission barrier. The reason is that, although the asymmetric degrees of freedom are very important in the actinide region, suppressing the second barrier by several MeV, the influence is much less significant in the SHE region. These degrees of freedom [26] are conveniently introduced in terms of the $P_3 + P_5$ terms in the nuclear potential as indicated above. The resulting potential energy surfaces in the ($\varepsilon_2$, $\varepsilon_4$) plane are shown in Fig. 16. We then introduce $\varepsilon(\varepsilon_4)$ as a new axis, representing symmetric distortions, and subsequently also $\varepsilon_3(\varepsilon_5)$, the coordinate of assymetry, the latter referring to a linear combination of $\varepsilon_3$ and $\varepsilon_5$. The new type of plot is shown in Fig. 17 for $^{236}$U in terms of $\varepsilon(\varepsilon_4)$ and $\varepsilon_3(\varepsilon_5)$. Fig. 18 is a photograph of a model constructed in softwood from the computer contour diagram in terms of these coordinates. Fig. 19 is a similar plot by the authors of ref. [2]. There $c$ and $h$ represent elongation and indentation, and $\alpha$ asymmetry.

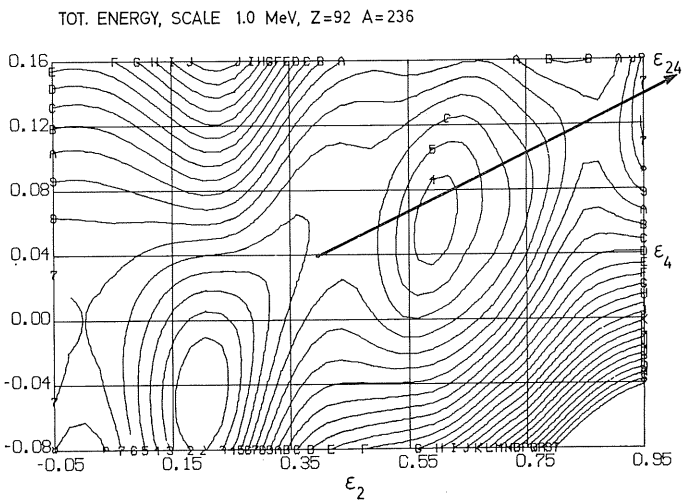


*Fig. 16.* Introduction of the coordinate $\varepsilon_{24}$, denoting corresponding elongation ($\varepsilon$) and waist-line ($\varepsilon_4$) shape coordinates along the valley of fission.

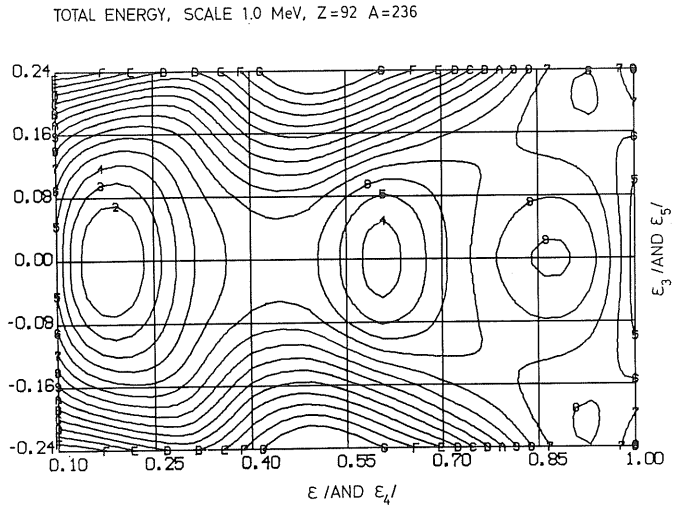


*Fig. 17.* Nuclear potential-energy surface for $^{236}_{92}$U in terms of $\varepsilon_{35}$, $\varepsilon_{24}$, here denoted "$\varepsilon$ (and $\varepsilon_4$)" and the asymmetry coordinate, here denoted "$\varepsilon_3$ (and $\varepsilon_5$)". The ground state is shown to the left. The "path to fission" is symmetric all the way to the second barrier, where there is a 2 MeV gain due to asymmetry.

## 8. Axial asymmetry

In the above discussion of nuclear shapes only deformations that preserve rotational symmetry have been included. There are, however, strong indications in particular from the end of the rare-earth region of the importance of the degrees of freedom of axial asymmetry. For the problem of the fission barrier these degrees of freedom were first taken into consideration by Pashkevich [27] and by Schultheiss and Schultheiss [28].

Recently Larsson et al. [29] have added a term proportional to $\varepsilon \sin\gamma(Y_{22} + Y_{2-2})$ to the potential above while modifying the $\varepsilon Y_{20}$ term to $\varepsilon \cos\gamma Y_{20}$. In this way for $\gamma = 0$ the rotationally symmetric prolate is restored while for $\gamma = 60$ in the pure ellipsoidal case a rotationally symmetric though oblately shaped potential is generated.

The influence of the gamma degree of freedom on the fission barriers in the actinide elements is strongest for the heavier ones. Similar results have recently been obtained by Götz et al. [30].

## 9. Barrier characteristics

With the inclusion of the asymmetric degrees of freedom we have obtained a considerable lowering of the second saddle points for actinide elements. Similarly the inclusion of the gamma degree of freedom serves to lower the first barrier. Both effects tend to improve the agreement with experiments. It may be appropriate to summarize, on the one hand the theoretical, on the other hand the experimental, information as to the heights of the two barrier peaks. This is done in Figs. 20 (first barrier) and 21 (second barrier).

The experimental data have been collected by S. Björnholm and E. Lynn [32]. The theoretical results represent those obtained in ref. [29].

The role of gamma in the super-heavy element region is similar to that for the actinides and causes a reduction of the inner barrier by up to 1.5 MeV as seen in Figs. 22 and 23 and Table I.

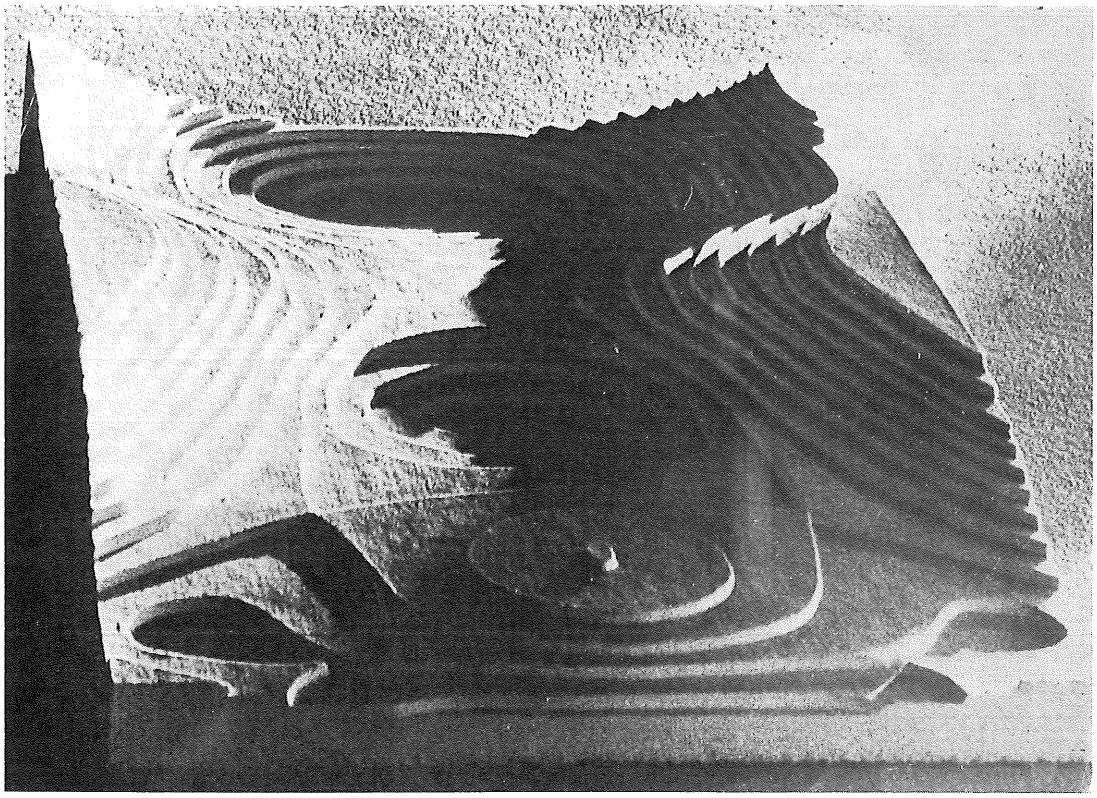

*Fig. 18.* A three-dimensional model surface corresponding to Fig. 17.

## 10. The super-heavy element half-lives

In order fully to understand the stability properties of SHE:s we must, in addition to the properties of their potential energy surfaces, also know the mass parameters and the dissipation associated with motion in the potential energy landscape. Concerning the dissipation practically nothing is known except for some very crude estimates based on experimental information [32]. Consequently the dissipation term in the collective Hamiltonian has been neglected in all calculations up to now. Moreover, the mass parameters are most often treated in a rather crude semiempirical approximation and even the few [33, 2] more detailed calculations, based on the cranking model, that have been performed involve a number of approximations, the appropriateness of which is difficult to evaluate.

From the potential energy surface and the mass parameters the fission half-lives are usually estimated by a semiclassical approximation leading to the following expression for the one-dimensional penetration.

$$t_{\frac{1}{2}} \propto \mathrm{e}^{-\frac{2}{\hbar}\int_{\varepsilon'}^{\varepsilon''}\sqrt{2|E-W(\varepsilon)|\,B(\varepsilon)}\,\mathrm{d}\varepsilon}$$

where the two end points $\varepsilon'$ and $\varepsilon''$ correspond to the entrance into the sub-barrier region and the exit on the other side of the potential barrier, respectively. $E$ is the energy of the collective

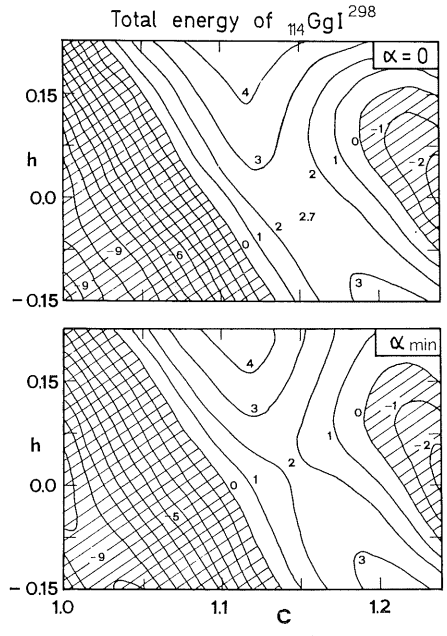


*Fig. 19.* Influence of the asymmetry parameter $\alpha$ in the calculations of ref. [2]. The agreement between the results of the different refs. as to the asymmetry effects is remarkable.

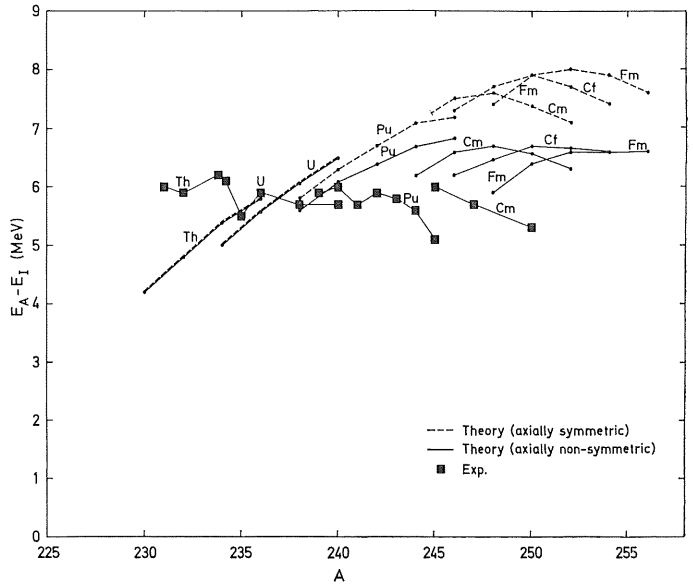


*Fig. 20.* The height of the inner barrier experimentally and theoretically. Note the much improved agreement when $\gamma$ is included.

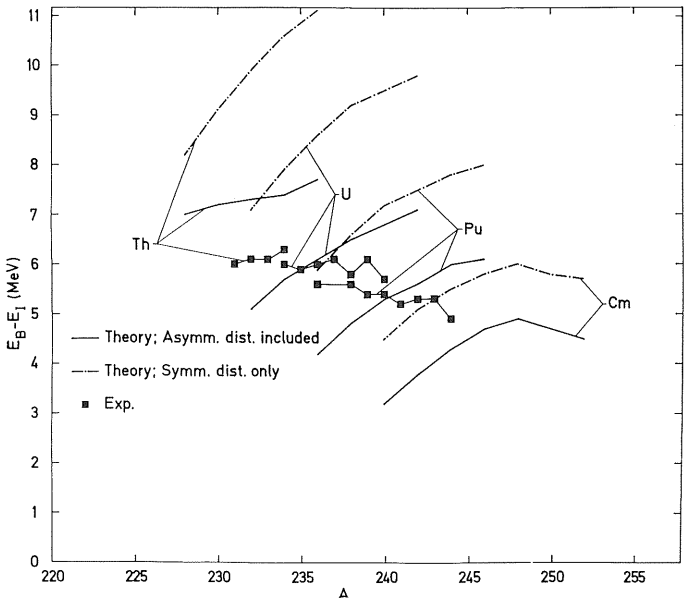


*Fig. 21.* The height of the second barrier experimentally and theoretically. Note the improved agreement when asymmetry is included.

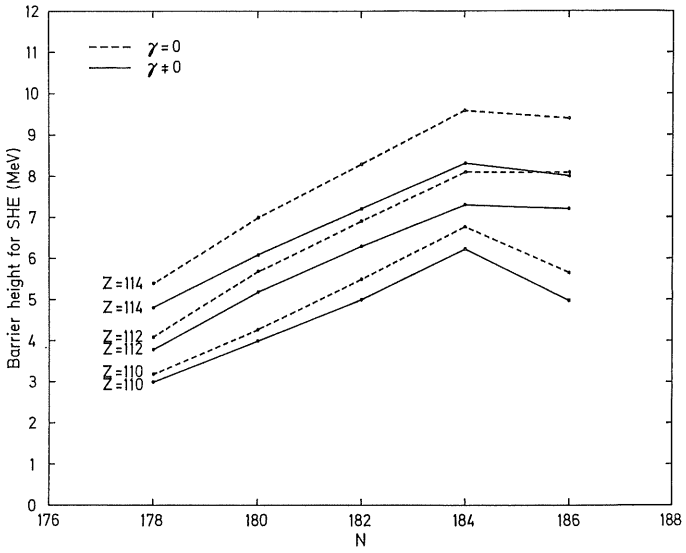


*Fig. 23.* Plot of the height of the inner (highest) barrier for a sequence of superheavy elements as a function of the neutron number. (Private communication from S. E. Larsson.)

motion and $W(\varepsilon)$ and $B(\varepsilon)$ are the potential energy and the mass parameter, respectively. As the mass parameter enters exponentially in the expression for the half-lives, small changes in the mass parameter may lead to a substantial change in the estimated half-lives.

The early calculations of the Lund–Berkeley–Warsaw group contained in ref. [9] predicted an island of SHEs as of Fig. 24. The fission half-life determinations also depend strongly on the capability of calculating good potential-energy surfaces, i.e. proper barriers. These barrier calculations have been carried through for the more sophisticated types of potentials by Brack et al. [2] and by Bolsterli et al. [34]. While the 1968 fission barrier comes out 10 MeV high for $^{298}114$, the latter authors obtain barrier heights of almost 13 MeV. Indeed the authors of ref. [2] also end up with fission half-lives of up to $10^{30-45}$ years where the 1968 calculations gave $10^{14}$ years or so. As mentioned above a large factor in the half-life estimates reflects on what is assumed about the mass parameters. Bolsterli et al., on the other hand, who use semiempirical inertial parameters, extrapolated from the actinide region, find fission half-lives

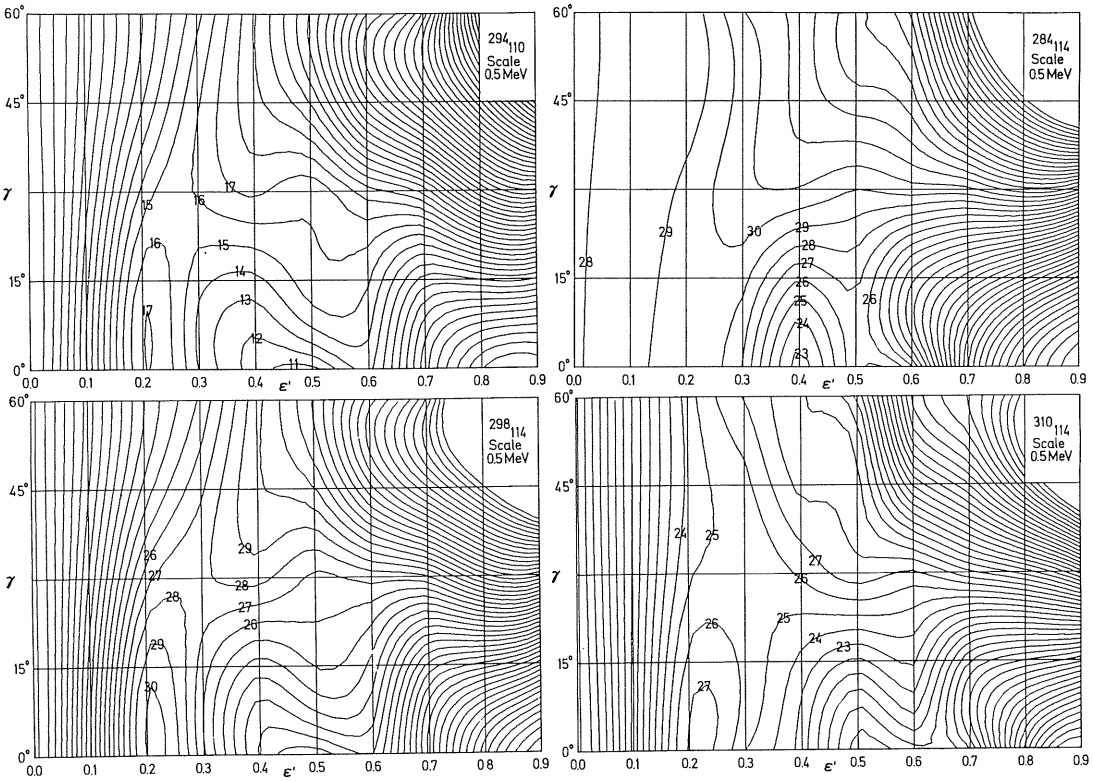


*Fig. 22.* Potential-energy surfaces for a few sampled superheavy elements in terms of $\varepsilon$ and $\gamma$. Note that the reduction due to $\gamma$ essentially only affects the inner barrier. Note furthermore the inherent deficiencies in the plot at $\varepsilon=0$. The minimum for the spherical case corresponds to the entire $\gamma$-axis. The equipotential lines are labeled by the computer program in units of 0.5 MeV such that lowest contour line corresponds to "1". Note that the nucleus $^{284}114$ is deformed in its ground state, while the other superheavy exhibited nuclei have spherical ground states. The reduction of the first barrier for instance for $^{298}114$, near $\varepsilon=0.2$, can be counted off from the figure as approximately 1.5 MeV. (Private communication from S. E. Larsson.)

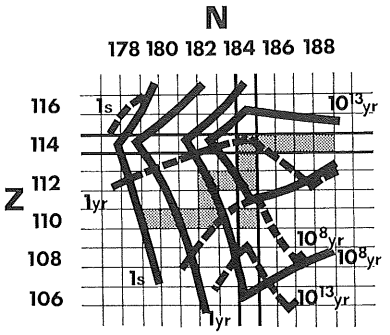


*Fig. 24.* Diagram of half-lives with respect to fission and alpha-decay as of ref. [9]. Beta-stable elements are denoted by cross-shadowed squares. Note that theoretically $^{294}110$ is the most favourable case (though barely beta-stable). Other good candidates are $^{296}112$ and $^{292}110$.

in gross agreement with those obtained in ref. [9] although somewhat longer, see Fig. 25. For the selective prediction of the nucleus with the longest total half-life with respect to fission, alpha and beta decay Bolsterli et al. support our early finding that $^{294}110$ is the most stable of the SHE nuclei. They estimate the total half-life to $10^{9.4}$ years, which figure differs by only a factor of 10 from our estimate. As pointed out already, the difference in the estimates of barrier heights reflects the selection of a nuclear mass region where parameters are effectively fitted and the different mass and distortion dependence of the spin-orbit term assumed for the two types of potentials compared. The different predictions as to the size of the $Z=114$ and $N=184$ gaps may be compared in Figs. 2 and 3. In view of these many uncertainties it is actually surprising to which degree the predicted fission half-lives agree among each other. It appears reasonably probable that the most long-lived SHE calculated should have a half-life of the order of millions of years. This internal agreement among the theorists is hard to reconcile with the fact that any SHEs have not yet been found. As we shall see later, however, recent calculations indicate that they may not be produced in nature. Furthermore, due mainly to the following three factors they are probably very difficult to produce in the laboratory.

1. Owing to the very narrow potential minimum in the deformation degrees of freedom (see Figs. 14*a*, *b*) the production process must lead to a very nearly spherical system or else the compound nucleus might fission immediately.

2. Dissipation processes may lead to very small production cross-sections [35].

3. Some recent calculations [36] indicate that the shell-effects (leading to increased stability of the ground states of the SHEs) are washed out with rising excitation energy. To be favourable the production process should produce the nuclei in low-lying excited states, a condition that is not easily met experimentally.

### 11. On the termination of the r-process path

Actually $^{244}$Pu with a half-life of 80 million years (or nearly the same as that predicted for $^{294}110$ by the authors of ref. [9]) was recently detected by chemical means from terrestial ores by the Los Alamos nuclear chemists. In case the truth is closer to the predictions by the authors of ref. [2] than to the predictions of the Lund–Berkeley–Warsaw group, it appears probable that the r-process of element synthesis, which is considered responsible for the terrestial quantities of $^{244}$Pu, $^{238}$U etc., fails to make anything but very small quantities of SHEs. To look a little into that problem R. Boleu et al. [37] have been studying fission barriers for very neutron-rich actinide elements, over a range of $N$ values extending from about 160 to and beyond 190. The predictions turn out to be very sensitive first to the choice of shell model potential responsible for the $N=184$ gap but also to the knowledge of the liquid-drop parameters, in particular to the value of the surface-symmetry term.

In the Myers–Swiatecki Lysekil version [22] of the liquid-drop model the parameters are fitted not just to reproduce masses but also to give reasonable fission barriers for actinide elements as well as for some elements lighter than Pb. In particular the difficulty in determining the surface symmetry term may be taken as a measure of the arbitrariness in this fitting procedure.

The surface symmetry coefficient $\varkappa_s$ is chosen by Myers–Swiatecki as 1.78 or equal to the volume symmetry coefficient. Seeger [36] instead determines the surface symmetry term independently, fitting masses only and not barriers, and ends up with a surface symmetry coefficient that in the MS formulation would correspond to $\varkappa_s=2.53$. We have now as an alternative (and also as a measure of our ignorance) used the large surface symmetry coefficient in a variant of the calculations. This must obviously result in a lowering of the actinide barriers as the surface energy is weakened. In order to retain the observed actinide barriers we have replaced the assumption of $G$ being proportional to the surface area with the assumption of $G=$ constant, an assumption which may reproduce better the more recent interpretation of data as to the level density above the highest of the fission barrier peaks. By this second parameter set, approximately the same barriers are obtained for the actinides.

The picture is significantly changed, however, for the neutron rich nuclei on the r-process path. The reduction due to the change in $\varkappa_s$ is thus considerable even when the compensatory change in the assumption about the pairing matrix element is introduced at the same time. The corresponding estimated fission half-lives are given in a critical region of the r-process path in Figs. 26 and 27.

In Fig. 26 (corresponding to $G \propto S$ and $\varkappa_s=1.78$) the following

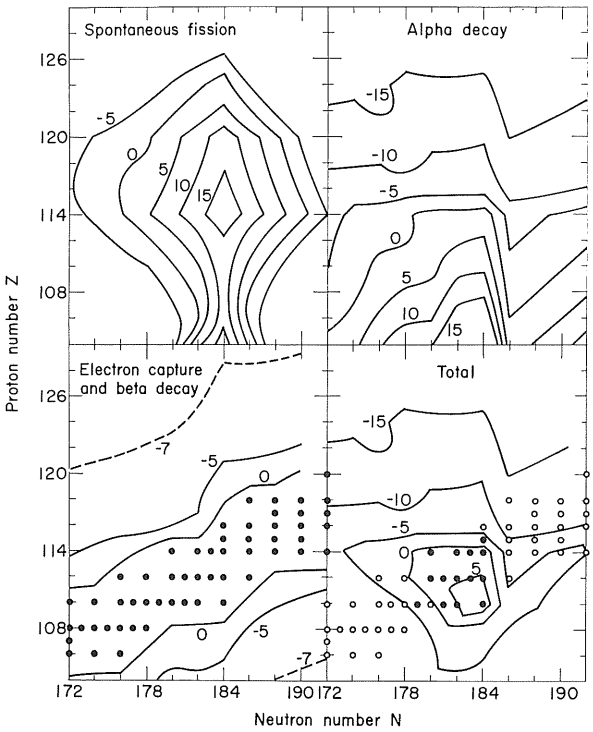


*Fig. 25.* Ten-logarithms of fission, alpha- and beta-decay and total half-lives in years in the $Z=114$, $N=184$ region according to ref. [3].

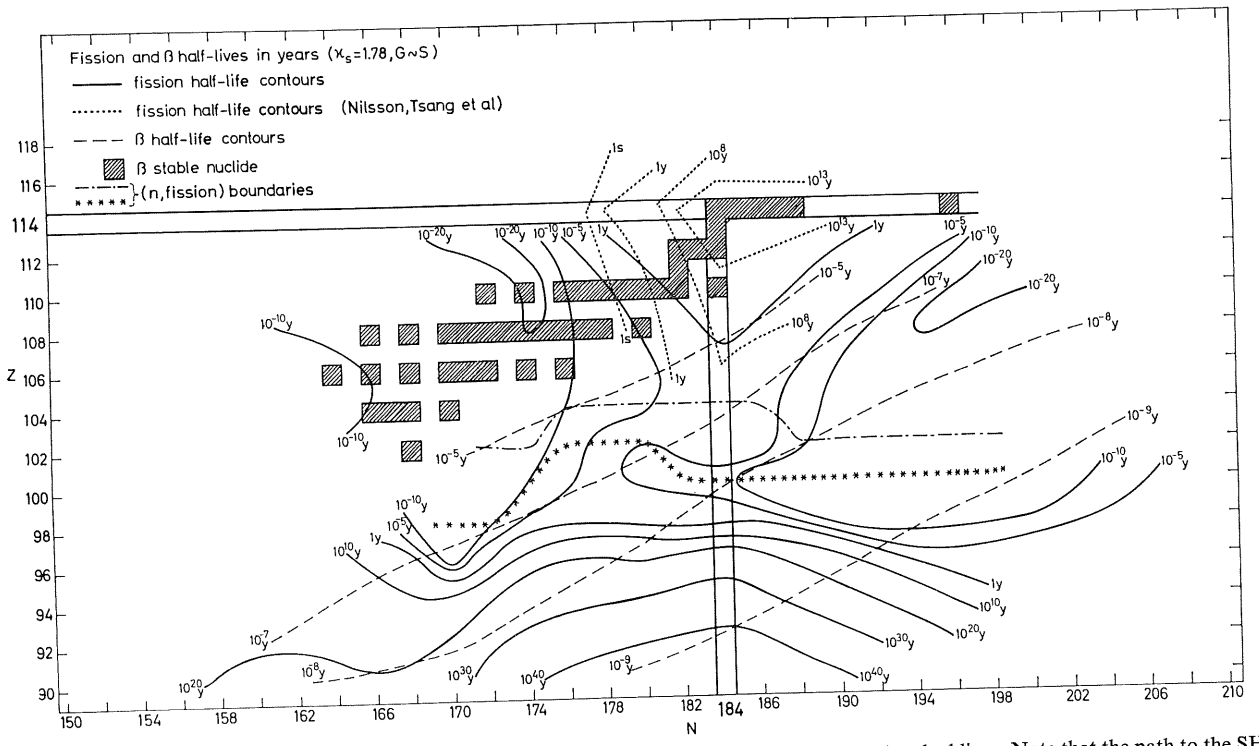


*Fig. 26.* Theoretical half-lives of elements calculated by R. Boleu [37] on the basis of the present model, containing the usually assumed r-process path elements, with respect to spontaneous fission (solid lines), beta-decay (dashed lines). Beta-stable elements in regions calculated are given by shaded squares. Limiting lines for dominance of neutron-induced fission over gamma decay according to two variants described in the text are marked by dot-dashed and cross-hatched lines. Note that the path to the SHE island appears impassable. The corresponding calculations are based on the assumptions that $G$ is proportional to surface area and the surface-symmetry coefficient $\varkappa_s = 1.78$. Note that the results exhibited in this figure are somewhat preliminary.

decay processes have been included, spontaneous and induced fission, alpha- and beta decay. Of these processes alpha half-lives are too long to affect the region of r-process nuclei and are neglected in the figure. Spontaneous fission half-lives are indicated by solid lines. The $10^{-10}$ $y$ (0.003 s) isochrone appears to terminate the r-process path at $Z \simeq 98$, $N \simeq 190$, from which point the subsequent beta-decay process (with half-lives marked by dashed lines) fails to reach the superheavy island as fission half-lives are shorter than beta half-lives somewhere along the beta decay path. Any progress along the thin bridge of half-lives in excess of $10^{-5}$ $y$ appears blocked by a line referring to induced fission. Along this line induced fission half-lives equal the half-lives of gamma-decay back to the ground state following neutron capture (two alternative lines, denoting "optimist" and "pessimist" estimates are indicated, both effectively blocking the passage). One might otherwise have imagined processes involving two subsequent neutron showers broken off by a short time interval (1–10 s) where beta-decay dominates. Similar two-step

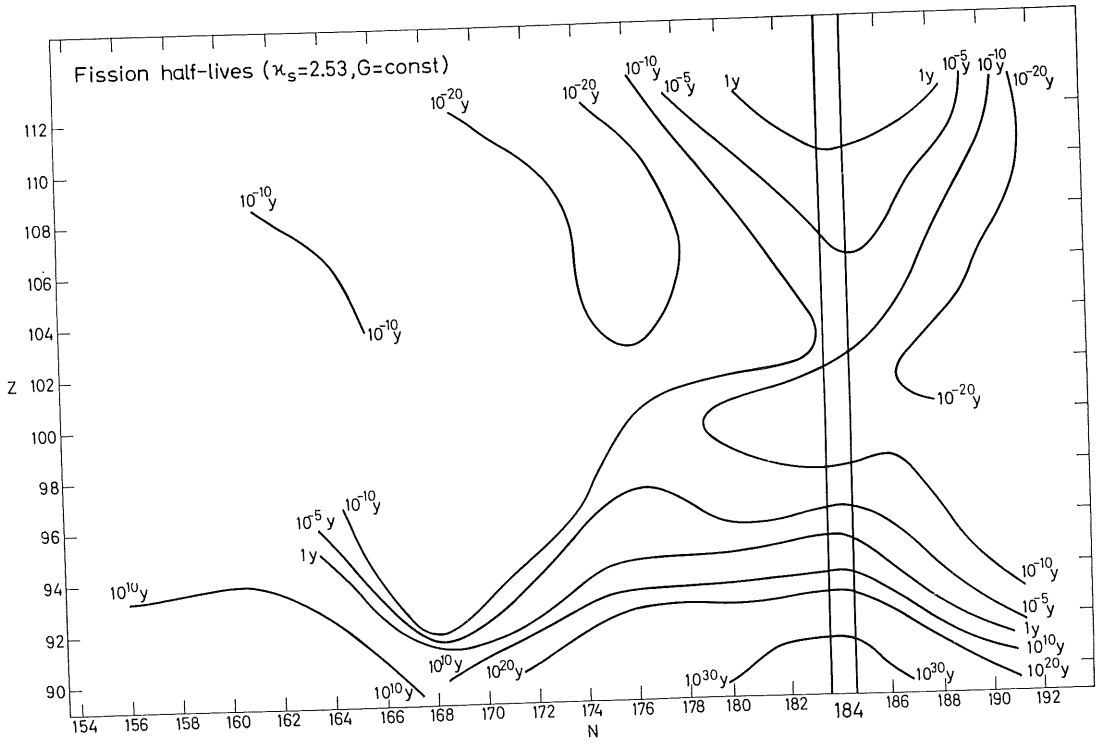


*Fig. 27.* Fission half-lives calculated for the alternative assumption to that employed in Fig. 26 $G$ = const. and $\varkappa_s$ = 2.53. Note the generally shorter half-lives relative to Fig. 26.

neutron showers from nuclear devices have recently been suggested by Meldner [39] for the artificial generation of superheavy elements.

Similar S.F. half-life estimates for the alternative $\varkappa_s$ assumptions are exhibited in Fig. 27 resulting in even shorter half-lives.

The asymmetry effect is not included in these estimates. From the available examples studied it appears that the reduction due to asymmetry can be expected to give rise to a reduction factor between $10^2$ and $10^5$. The inclusion of this effect would thus make the r-process path terminate for even smaller $A$-values.

It must be emphasised, that the conclusions obtained are as mentioned sensitive to the estimate of the shell correction energy connected with $N=184$. The latter gap comes out smaller on the basis of the modified oscillator model than in terms of other single-particle potentials employed (see Fig. 3).

The r-process path recently suggested by Schramm and Fowler [40], predicting a probable population of the SHE island by the r-process, was based on fission and alpha half-life estimations in terms of semiempirical half-life formulas. The shell correction term entering the effective fissility value $x$ is partially based on empirical information on shell energies available in the actinide region, while for the extrapolation to the superheavy region the results of the 1968 calculations [9] have been utilized. Our recent calculations, here referred to, cast considerable doubt on the procedure followed. Such an effective fissility value is hardly sufficient to reproduce the complex features of a two- or three-peak barrier.

## 12. Conclusions

The prediction of half-lives of superheavy elements rests at the present time first on the applicability of the microscopic-macroscopic approach developed by Swiatecki and Strutinsky. The shell correction method of the latter author now appears reasonably well founded. The results are also borne out by alternative methods now being explored. Secondly, it rests on the detailed knowledge of the liquid-drop constants and the applicability of those in a new mass region. Thirdly, and most critically, the predictions depend on the availability of a single-particle model the parameters of which may be reliably extrapolated to a new mass region.

The magnitude of the $Z=114$ and $N=184$ shell gaps are predicted somewhat different according to the different single-particle models now in use. As a consequence of this the predicted fission and (to a minor extent) alpha half-lives differ by several orders of magnitude.

The details of the superheavy island are thus subject to considerable doubt. On the other hand, if the concept of "existence" of a superheavy island is defined as the total half-life of at least one element being longer than, say, 1 day, the probability for this to occur is very large a priori, as it requires essentially only that there is a subshell effect large enough to establish a ground state spherical minimum and thus to break the tendency to ground state prolate deformation persistent among the actinide elements. In addition this shell effect may occur in terms of either $N$ or $Z$ or both. For $Z>150$ not even very strong shell effects (the $Z=164$ shell may indeed be a very strong shell closure) appear to be large enough to overcome the Coulomb repulsion which latter is dominant for these high-Z values.

## Acknowledgements

We are indebted to our co-workers R. Bengtsson, R. Boleu, S. E. Larsson and P. Möller for helping us to collect the most recent information on the subject and supplying us with their unpublished results. We are grateful to J. R. Nix for kindly sending unpublished material and generously sharing his views on the subject.

## References

1. Johansson, T., Nilsson, S. G. and Szymanski, Z., Ann. Phys. Paris **5**, 377 (1970).
2. Brack, M., Damgaard, J., Jensen, A. S., Pauli, H. C., Strutinsky, V. M. and Wong, C. Y., Rev. Mod. Phys. **44**, 320 (1972).
3. Nix, J. R., Ann. Rev. Nucl. Sci. **22**, (1972), in press.
4. Bassichis, W. H., Kerman, A. K., Tsang, C. F., Tuerpe, D. R. and Wilets, L., Livermore Preprint UCRL-73044 (1971), to be published; Bassichis, W. H. and Wilets, L., Phys. Rev. Lett. **22**, 799 (1969).
5. Vauterin, D., Vénéroni, M. and Brink, D. M., Orsay Preprint IPNO/TH 193 (1970).
6. Köhler, H. S., Nucl. Phys. **A 162**, 385 (1971); Nucl. Phys. **A 170**, 88 (1971).
7. Vauterin, D., Vénéroni, M. and Brink, D. M., private communication, 1971.
8. Ragnarsson, I. and Nilsson, S. G., Proc. Colloq. Transitional Nucl. Orsay, 30 June – 2 July 1971, p. 112. Institut de Physique Nucléaire d'Orsay, 1972.
9. Nilsson, S. G., Tsang, C. F., Sobiczewski, A., Szymanski, Z., Wycech, S., Gustafsson, C., Lamm, I.-L., Möller, P. and Nilsson, B., Nucl. Phys. **A 131**, 1 (1969).
10. Swiatecki, W. J., Proc. 2nd Int. Conf. on Nuclidic Masses, Vienna, 15–19 July, 1963 (ed. W. H. Johnston, Jr.), p. 58. Springer Verlag, 1964.
11. Strutinsky, V. M., Yad. Fiz. **3**, 614 (1966), Sov. J. Nucl. Phys. **3**, 449 (1966).
12. Strutinsky, V. M., private communication, 1971.
13. Andersen, B. L., Dickmann, F. and Dietrich, K., Nucl. Phys. **A 159**, 337 (1970).
14. Holzer, P., Mosel, U. and Greiner, W., Nucl. Phys. **A 138**, 241 (1969).
15. Johansson, T., Nucl. Phys. **A 183**, 33 (1972).
16. Slavov, B., Galonska, J. E. and Faessler, A., Phys. Lett. **37B**, 483 (1971).
17. Bohr, A. and Mottelson, B., Nuclear Structure, vol. 2 (to be published). Benjamin, W. A. Inc., New York.
18. Ramamurthy, V. S., Kapoor, S. S. and Kataria, S. K., Phys. Rev. Lett. **27**, 386 (1970); Huizenga, J. R., Proc. Int. Conf. Stat. Prop. Nucl. Albany, Aug. 1971, to be published.
19. Moretto, L. G., Phys. Lett. **38B**, 393 (1972).
20. Bengtsson, R., Nucl. Phys., in press.
21. Tsang, C. F., Berkeley Report UCRL-18899 (1969).
22. Myers, W. D. and Swiatecki, W. J., Proc. Int. Symp. Why How Investigate Nuclides Far off Stability Line, Lysekil, 21–27 Aug. 1966, p. 343, Almqvist and Wiksell, Stockholm, 1967.
23. Mosel, U. and Schmitt, H. W., Nucl. Phys. **A 165**, 73 (1971).
24. Pashkevich, V. V., Nucl. Phys. **A 169**, 275 (1971).
25. Adeev, G. D., Cherdantsev, P. A. and Gamalya, I. A., Phys. Lett. **35B**, 125 (1971).
26. Möller, P. and Nilsson, S. G., Phys. Lett. **31B**, 283 (1970).
27. Pashkevich, V. V., Nucl. Phys. **A 133**, 400 (1969).
28. Schultheiss, H. and Schultheiss, R., Phys. Lett. **34B**, 245 (1971).
29. Larsson, S. E., Ragnarsson, I. and Nilsson, S. G., Phys. Lett. **38B**, 269 (1972).
30. Götz, U., Pauli, H. C. and Junker, K., Phys. Lett. **39 B**, 436 (1972).
31. Bjørnholm, S. and Lynn, J. E., private communication, 1970.
32. Bjørnholm, S., Copenhagen Preprint, 1971.
33. Sobiczewski, A., Szymanski, Z., Wycech, S., Nilsson, S. G., Nix, J. R., Tsang, C. F., Gustafsson, C., Möller, P. and Nilsson, B., Nucl. Phys. **A 131**, 67 (1969).
34. Bolsterli, M., Fiset, E. O., Nix, J. R. and Norton, L., Phys. Rev. **C 5** 1050 (1972).
35. Swiatecki, W. J., Berkeley Preprint LBL-549, 1971.
36. Moretto, L. G., Nucl. Phys. **A 182**, 641 (1972).
37. Boleu, R., to be published; Boleu, R., Nilsson, S. G., Sheline, R. K. and Takahashi, K., Phys. Lett. **40B**, 517 (1972)
38. Seeger, P. A., Los Alamos Preprint LA-DC-12792, 1971.
39. Meldner, H. W., Phys. Rev. Lett. **28**, 975 (1972).
40. Schramm, D. N. and Fowler, W. A., Nature **231**, 103 (1971).